

Melting the roof of a chamber containing a hot, turbulently convecting fluid

By **HERBERT E. HUPPERT**

Department of Applied Mathematics and Theoretical Physics, University of Cambridge,
Silver Street, Cambridge CB3 9EW, UK

AND **R. STEPHEN J. SPARKS**

Department of Earth Sciences, University of Cambridge, Downing Site,
Cambridge CB2 3EQ, UK

(Received 29 June 1987)

The input of a hot, turbulently convecting fluid to fill a chamber can result in the roof of the chamber melting. The rate of melting of the roof is here analysed experimentally and theoretically. Three separate cases are considered. The melt may be heavier than the fluid and initially sink through it. The intense motion in the fluid then mixes the falling melt in with it. Alternatively, the melt may be less dense than the fluid and form a separate layer between the roof and the fluid. This melt layer can itself be in quite vigorous convective motion. An intermediate case is shown to be possible, wherein the melt is initially denser than the fluid, and sinks. As its temperature increases and its density decreases, it becomes less dense than the surrounding fluid and rises. Experimental simulations of each of these three cases are described. The experiments employ a roof of either wax or ice which is melted by the aqueous salt solution beneath it. The second case, that of a light melt, has important geological applications. It describes the melting of the continental crust by the emplacement of a hot, relatively dense input of fluid basaltic rock. Both the basaltic layer and the resultant granitic melt layer crystallize and increase their viscosities as they cool. These effects are incorporated into the analysis and the rate of melting and the temperatures of the two layers are calculated as functions of time. The process is exemplified by the formation of the Cerro Galan volcanic system in Northwestern Argentina over the last 5 million years. An Appendix analyses the thermal history of the fluid in a chamber that does not melt and compares the results obtained with those derived previously.

1. Introduction

When hot fluid is introduced into a solid container, the heat may melt all, or part, of the container and permit the fluid to escape, with potentially disastrous consequences. The introduction of hot magma into a magma chamber surrounded by rock with relatively low melting temperatures is not as severe, in that the magma is not able to escape, but nevertheless the process is geologically important. The molten material originating from the initially solid surrounding rock can become mixed with the magma and contaminate it. Upon eruption, the composition of the magma will then be different from that when it first entered the chamber. This complicates the geologist's interpretation of the products of volcanic eruptions. Besides the geological applications, there are many other situations in which melting of retaining

boundaries, due to vigorous turbulent motion in the fluid, is important. This has motivated a combined experimental and theoretical study of the melting of a solid roof by the introduction of hot fluid beneath it. The molten material originating at the roof is referred to simply as the *melt*, in line with standard geological and metallurgical practice.

The experiments consisted of placing a wax roof at the top of a Perspex container of rectangular cross-section. A hot aqueous solution of salt was rapidly introduced near the base of the container until it was completely filled. The density of this hot solution could be varied by altering its composition. Thus three separate cases could be considered. First, the fluid density could be less than the melt density (for all temperatures in the relevant range). In this case the melt initially sank, but the turbulent motion resulting from the heat transfer to the cold roof quickly mixed the molten wax into the fluid (with which it was miscible). A photograph of a typical fluid/melt interface makes up figure 1(a). Second, the fluid density could exceed the melt density. The melt then formed a separate layer between the roof and the hot fluid. The layer was initially quiescent and transferred heat by conduction, though subsequently convection generally occurred. Figure 1(b) depicts a light melt layer which is in the latter state. Finally, an intermediate case was possible, in which the melt density at the melting point only slightly exceeded that of the hot fluid. The melt began to sink. As it did so its temperature rose and its density could decrease to be less than that of the fluid; streamers of melt would then rise. A photograph showing this bi-directional motion is reproduced in figure 1(c).

This simple experimental account was briefly outlined in Huppert (1986), which includes colour photographs of the experiments. The current paper presents, in §§2 and 3, theoretical analyses of the first two cases, guided by the experimental observations. Comparisons between the theoretical and experimental results for the first case will also be discussed. Both for the wax/aqueous-solution system described in the previous paragraph and for the melting of an ice roof into warm water, the agreement is quite good.

The situation of intermediate density will be very briefly surveyed in §4.

In the geological situation the contained magma crystallizes as it cools. This crystallization increases the amount of heat available to melt the surrounding rock owing to the latent-heat release. The crystals are typically so small that they tend to remain suspended in the turbulently convecting magma. The presence of the crystals increases the effective viscosity of the magma. A description of these effects and a discussion of the results for typical magmatic systems is presented in §5. A more detailed account, written for geologists rather than fluid dynamicists, appears in Huppert & Sparks (1988*a*), and an updated version is presented in Huppert & Sparks (1988*b*).

The material of the paper is complementary to earlier work analysing the melting of the substrate by a hot, turbulently flowing stream (Huppert *et al.* 1984; Huppert & Sparks 1985; Huppert 1986). They used the results to explain how the stream melts the floor and forms thermal erosion channels. In the geological context, after the stream ceases to flow, part of the fluid collects in ponds and will then cool and solidify. These processes were analysed quantitatively by Turner, Huppert & Sparks (1986) and successfully compared with laboratory experiments. The formulation developed in that paper acted as a foundation to the analysis employed here.

For comparison, a brief analysis of the situation in which the container does *not* melt is presented in the Appendix. The roof is assumed to be very thick and one of the questions addressed, which arose as an outcome of stimulating conversations

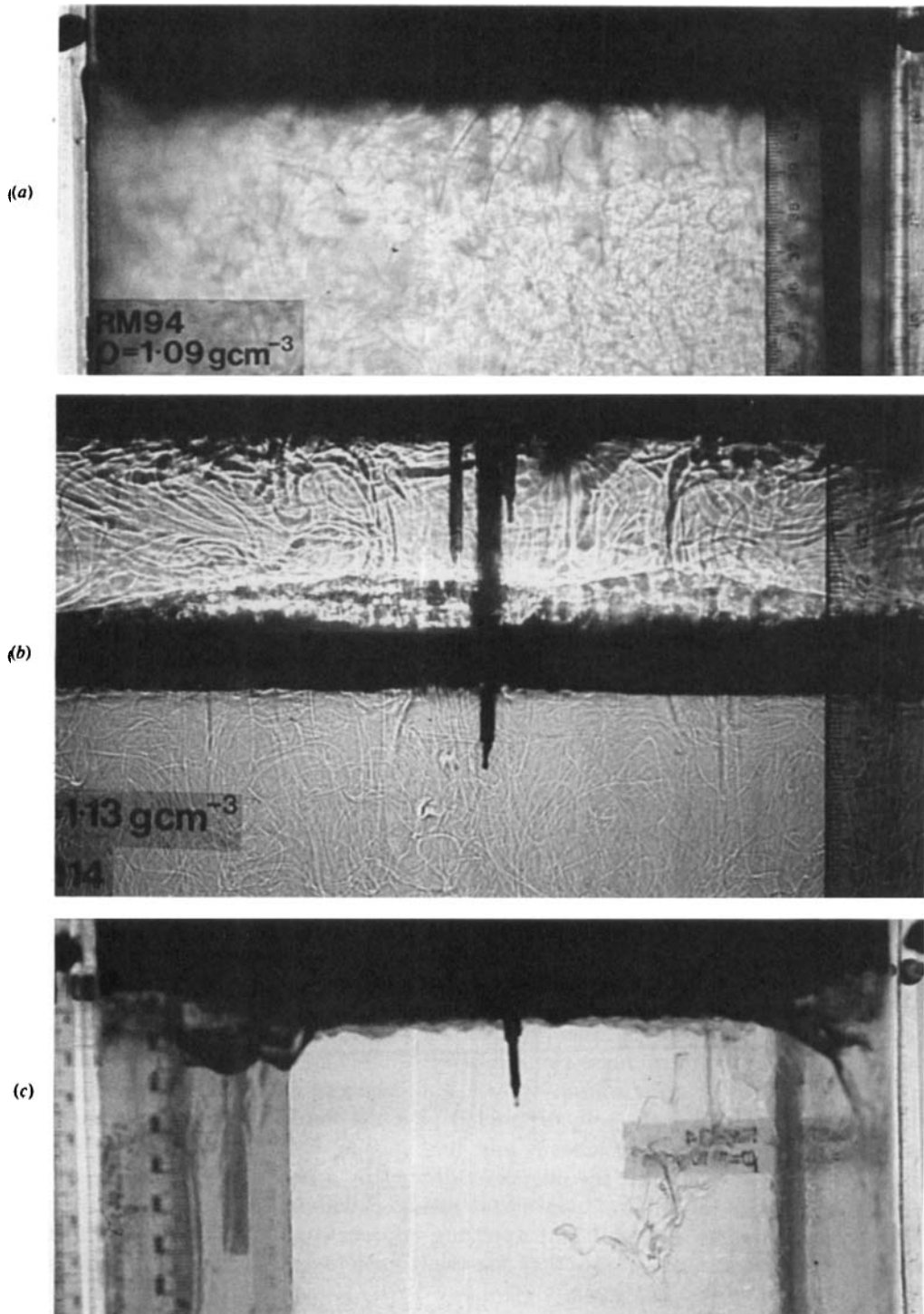


FIGURE 1. Photographs of the three different cases of a solid roof melting owing to the introduction of a hot, turbulently convecting fluid beneath the roof: (a) melt density exceeds fluid density, with melt and fluid being intimately mixed; (b) melt density is less than fluid density and the melt forms a separate layer between roof and fluid; and (c) melt density initially exceeds fluid density but as the melt falls through the fluid and warms, its density decreases to be less than the fluid density.

with Bruce Marsh, is the extent of the influence of thermal conduction in the roof on the intensity of convection in the fluid. An evaluation of this influence settles a geological controversy which is currently impeding progress. The presence of a thick solid roof causes the temperature at the boundary between the roof and the fluid to approach that of the fluid and thus decrease the intensity of the convection. However, if the initial Rayleigh number is sufficiently large, turbulent convection will still persist. We calculate the effective Rayleigh number (A 17), which must exceed a value of about 10^6 for turbulent motion to be maintained and also evaluate the various timescales of the thermal adjustment (A 10) and (A 12).

2. Heavy melt

Consider the layer of hot fluid to have initial temperature T_0 and vertical thickness D and assume that the solid roof above it is of very large thickness. For the case in which the melt mixes intimately with the fluid, we seek the subsequent mean temperature $T(t)$ of the fluid/melt mixture and its thickness $D+a(t)$ as functions of time. Figure 2 presents a sketch of the geometrical set-up. We assume that the problem can be considered as one-dimensional and that the thermal Rayleigh number of the fluid is sufficiently large that it convects turbulently. Then the heat flux F from the layer to the solid can be evaluated from the four-thirds relationship (Turner 1973)

$$F = \rho c J (T - T_m)^{\frac{4}{3}}, \quad (1)$$

where ρ is the fluid density, c the specific heat, T_m the melting temperature of the roof, and thus the temperature at the solid/melt interface, and

$$J = \gamma \left(\frac{\alpha g \kappa^2}{\nu} \right)^{\frac{1}{3}}, \quad (2)$$

where α is the coefficient of thermal expansion of the fluid, g the acceleration due to gravity, κ the thermal diffusivity, ν the kinematic viscosity, and γ a dimensionless constant. Denton & Wood (1979) survey recent experimental data at relatively high Rayleigh numbers and various Prandtl numbers which indicate that $\gamma \approx 0.10$ (in contrast to Turner's (1973) earlier suggestion based on experiments at lower Rayleigh numbers that $\gamma \approx 0.21$). Pure-heat-flux experiments that we have conducted with aqueous solutions support the former, lower value, which is hence used here. The influence of the mass flux from the roof is neglected in (1) on the assumption that the motion is dominated by the thermal transfers. The effect of the (neglected) compositional flux is to increase the intensity of the motion and augment the heat flux represented by (1). For simplicity, we shall here also neglect the variation in all physical properties as melt is incorporated into the fluid. However, variations in these properties with melt fraction, and hence time, could be incorporated in a straightforward manner and the effects evaluated by a numerical simulation.

The flux F melts the solid at a rate that can be calculated by solving the thermal diffusion equation in the solid and applying conservation of heat at the melting interface. With the assumption that the melt rate is quasi-steady, the diffusion equation can be solved analytically (Holman 1976; Huppert 1986) to yield

$$\dot{a} = \frac{F}{H_s} = A (T - T_m)^{\frac{4}{3}}, \quad (3a, b)$$

where

$$A = \frac{\rho c J}{H_s}, \quad H_s = \rho_s [c_s (T_m - T_\infty) + L], \quad (4a, b)$$

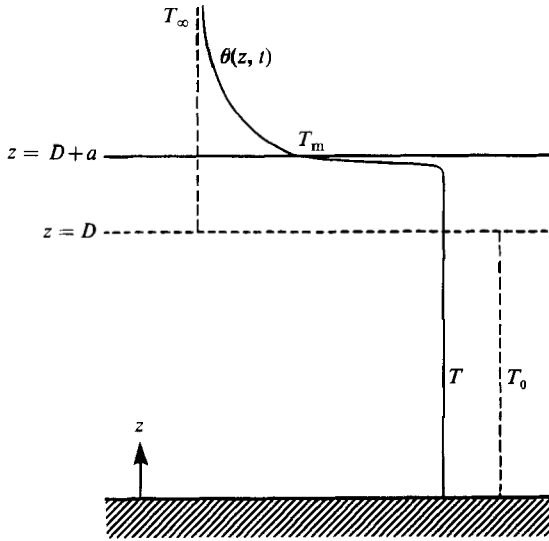


FIGURE 2. A sketch of the initial and subsequent geometry and mean temperature profile when the melt density exceeds the fluid density.

ρ_s is the density of the solid, c_s its specific heat, L its latent heat on melting and T_∞ the temperature in the solid far from the solid/melt interface. Equation (3a) states that the rate of melting is given by the ratio of the heat input F to the heat needed to bring the solid up to its melting temperature T_m from T_∞ and then to melt it. While (3) is only strictly valid if \dot{a} is constant, results obtained using it in this work were negligibly different from those obtained by solving the full diffusion equation. The use of (3), however, has the large advantage that analytical representations of the results can be obtained.

With the assumption that there is no heat loss from the base of the fluid, conservation of heat indicates that

$$\dot{a}(T - T_m) + (D + a)\dot{T} + J(T - T_m)^{\frac{4}{3}} = 0. \quad (5)$$

The first term of (5) represents the rate at which heat is used to raise the melt from the melt temperature T_m to that of the melt/fluid mixture T . The second term represents the rate at which the heat content of the melt/fluid mixture changes. The third term represents the heat flux from the mixture to the overlying roof.

Equations (3b) and (5), together with the initial conditions

$$T = T_0, \quad a = 0 \quad (t = 0), \quad (6a, b)$$

specify the problem. The introduction of the non-dimensional variables

$$\theta = \frac{T - T_m}{T_0 - T_m}, \quad (7a)$$

$$\eta = \frac{C}{D}a \quad (7b)$$

and

$$\tau = ACD^{-1}(T_0 - T_m)^{\frac{4}{3}}t, \quad (7c)$$

where

$$C = \frac{H_s}{\rho c(T_0 - T_m)}, \quad (8)$$

into (3)–(6) leads to

$$(C + \eta) \frac{d\theta}{d\tau} + \theta^{\frac{4}{3}} + C \theta^{\frac{4}{3}} = 0, \quad (9)$$

$$\frac{d\eta}{d\tau} = \theta^{\frac{4}{3}}, \quad (10)$$

$$\theta = 1, \quad \eta = 0 \quad (t = 0). \quad (11)$$

The one non-dimensional parameter, C involved in the solution represents the ratio of two quantities. The first is the heat required to bring solid of thickness D to its melting temperature and then melt it. The second is the initial heat content of the hot fluid with respect to the melting temperature of the roof.

Substituting (10) into (9), we obtain

$$\frac{d}{d\tau} [(C + \eta)\theta] + C \frac{d\eta}{d\tau} = 0, \quad (12)$$

the first integral of which, upon using (11), becomes

$$(C + \eta)\theta + C\eta = C. \quad (13)$$

Substituting (13) into (10), we obtain

$$\frac{d\eta}{d\tau} = C^{\frac{4}{3}}(1 - \eta)^{\frac{4}{3}}(C + \eta)^{-\frac{4}{3}}. \quad (14)$$

From (13) and (14) it can be seen that

$$\theta \rightarrow 0, \quad \eta \rightarrow 1 \quad (\tau \rightarrow \infty) \quad (15)$$

for all (positive) C . The interpretation of (15) is that eventually the temperature in the melt/fluid mixture approaches T_m , at which time all the initial excess heat content of the fluid has been used in producing the melt. In dimensional terms, a layer of thickness $C^{-1}D$ has been melted from the roof and incorporated into the fluid – a result that can be obtained directly by consideration of conservation of heat. Numerical solutions of (11), (13) and (14) are presented in figure 3.

An analytic solution can be found for large values of C . In that limit η can be neglected with respect to C in the first term of (13) and in the right-hand side of (14). The resulting equations have solutions

$$\theta = [1 + \frac{1}{3}t]^{-3} \quad (16)$$

and

$$\eta = 1 - [1 + \frac{1}{3}t]^{-3}. \quad (17)$$

The graphs in figure 3 indicate that (16) and (17) represent reasonable approximations for $C \geq 1$.

The experiments

We carried out a total of eight experiments with a wax roof and two with a roof made of ice. In all cases, the roof was made in a wooden mould of dimensions $20 \times 20 \times 15$ cm. When ready, the roof was lowered 10 cm into a thermally insulated Perspex container, to leave a $20 \times 20 \times 40$ cm high space beneath it. The wax used was

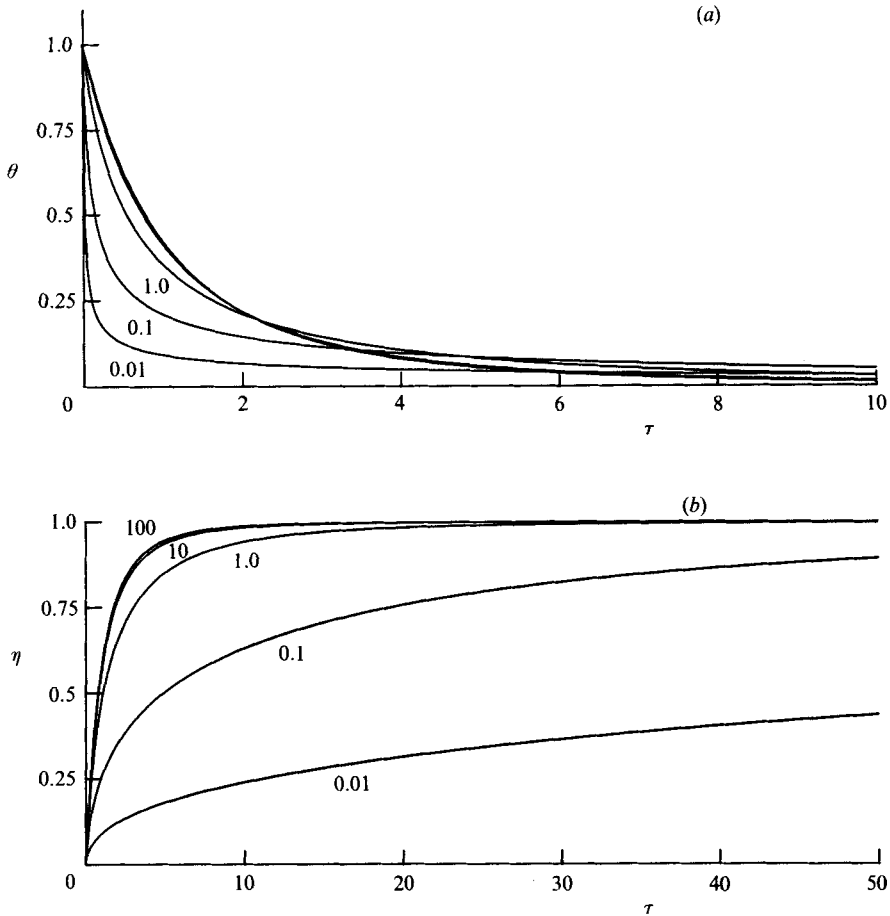


FIGURE 3. (a) The non-dimensional temperature $\theta = (T - T_m)/(T_0 - T_m)$ and (b) melt thickness $\eta = (C/D)a$ as a function of the non-dimensional time $\tau = (AC/D)(T_0 - T_m)^{3/2}t$ for $C = 0.01, 0.1, 1.0, 10$ and 100 .

polyethylene glycol, PEG 1000, which is miscible with water and has a melting temperature range of 37–40 °C. Calibrations that we conducted indicate that the density of the solid wax is 1.21 g cm⁻³ at room temperature and decreases in the molten state fairly linearly between 1.109 g cm⁻³ at 40 °C to 1.097 g cm⁻³ at 55 °C as shown in figure 4. Also shown in the figure are the densities of the various aqueous solutions used in the experiments. All the solutions were introduced at approximately 70 °C, with small amounts of solution added periodically at the base of the container so as to compensate for the decrease in volume as the fluid cooled. The fluid level was in this way maintained in contact with the base of the wax. The experiments were monitored until most of the wax had melted, by which time the temperature in the solution had fallen by some 10–15 °C. Movie sequences were shot during three of the experiments.

In most of the experiments we measured temperatures from a thermistor array. Typically five thermistors were initially frozen into the solid wax and another three were positioned at different heights in the solution. At any instant the readings of these latter three thermistors were essentially identical, as were the readings in the other thermistors after they were surrounded by solution owing to the melting of

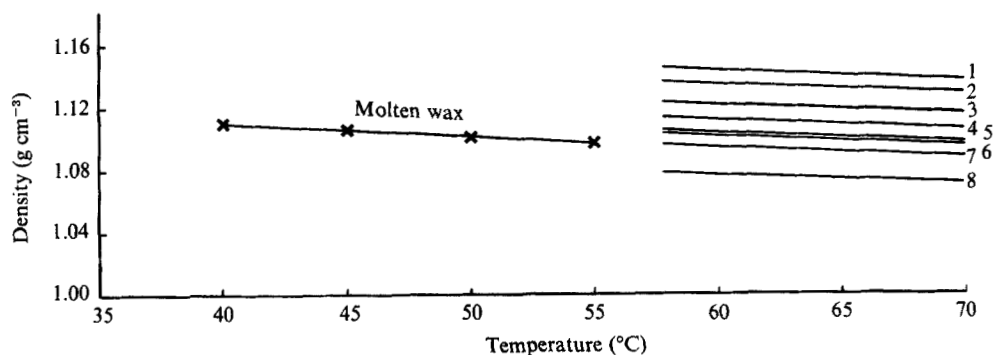


FIGURE 4. The density of molten polyethylene glycol 1000 and the densities of the aqueous solutions in the eight experiments that we performed as a function of temperature over the temperature range of the experiments.

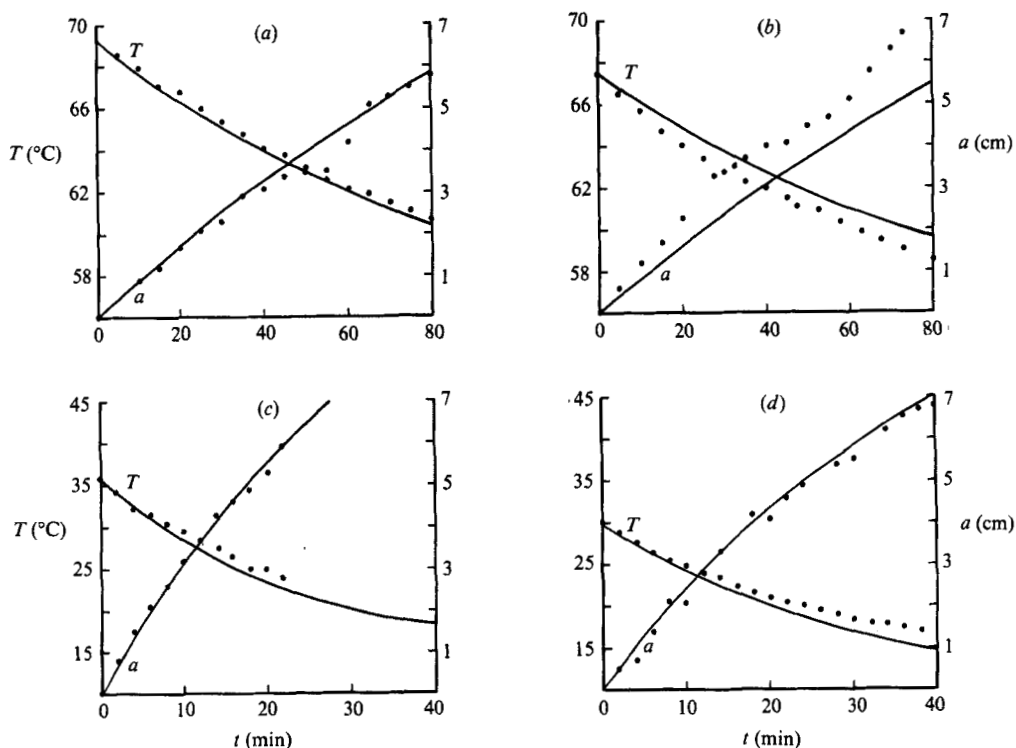


FIGURE 5. Experimental (.) and theoretical (—) temperatures and melt thickness as functions of time: (a) depicts the results of experiment 7; (b) experiment 8; (c) and (d) the experiments with an ice roof.

adjacent wax. This confirms the idea, incorporated into the theoretical analysis, that the temperature in the body of the solution was uniform. As the wax melted, the retreating base of the solid block became slightly uneven, as indicated in figure 1 (a). Nevertheless, a measurement of the 'mean' height of the base could be taken fairly reliably by eye. The results from two experiments, 7 and 8, are depicted in figure 5 (a, b), which also graphs the corresponding theoretical result obtained from the numerical integration of (11), (13) and (14). The agreement is seen to be quite good.

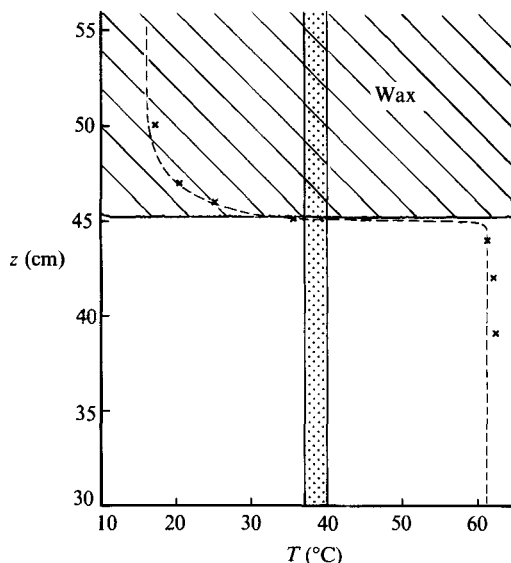


FIGURE 6. Experimental (\times) and theoretical (---) temperature against height for experiment 7 after 60 min. The solid line at 45.2 cm represents the observed base of the wax. The stippled region represents the melting range of the wax.

Figure 6 displays a typical series of temperature readings, taken after experiment 7 had progressed for 60 min, and includes the corresponding theoretical curve. The visual observation of the base of the wax is also shown and agrees to within a few millimetres with the position that would be predicted from the temperature profile only.

We thought that it might also be interesting to carry out some experiments on an ice roof melting into warm water. It might be suggested that because of the density relationship of water as a function of temperature, with a maximum density around 4°C , the theoretical analysis would not be relevant. On the other hand, it could be argued that as long as the density in the body of water beneath the ice was well below the density at 0°C , the detailed density relationship would not have an effect in the turbulent flow. This proved to be the case. Figure 5(c, d) presents data on the water temperature and thickness of melt as functions of time for the two experiments. Also plotted are the appropriate numerical solutions of (11), (13) and (14). The agreement between the observed and theoretical results is quite satisfactory.

3. Light melt

If the melt density is less than the fluid density, it will form a separate layer between the roof and the hot fluid. Initially the Rayleigh number in this intermediate layer will be less than the critical value necessary for convection and the melt will transfer heat only by conduction, even though the fluid beneath it is in vigorous turbulent motion. There may be a weak transfer of material across the interface, by the entrainment mechanisms reviewed by Turner (1973, Ch. 9), but we neglect this influence here. It was not detected in any of our experiments.

Let $T(t)$ denote the mean temperature of the hot fluid, and $T_1(t)$ that at the base of the melt layer, whose thickness will be denoted by $a(t)$, as sketched in figure 7(a).

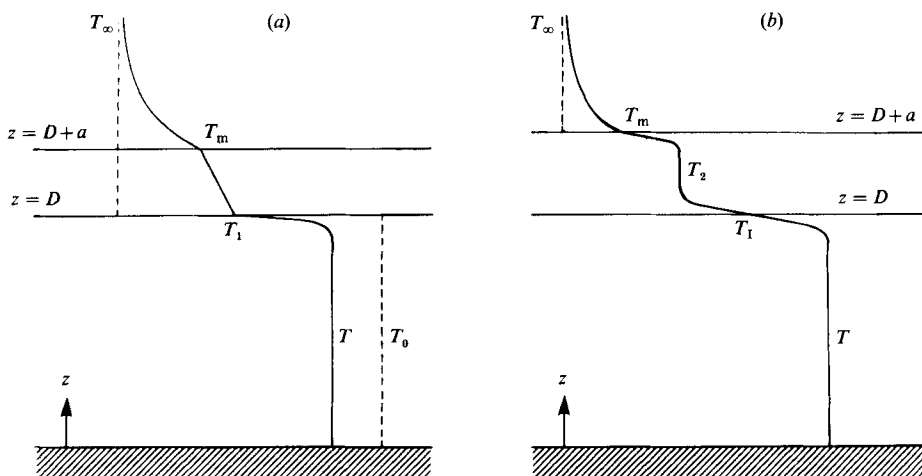


FIGURE 7. A sketch of the initial and subsequent geometry and mean temperature profiles when the melt, whose density is less than the fluid density, is transferring heat (a) by conduction, and (b) by turbulent convection.

These functions represent the three unknowns that describe the state of the system. In terms of them the heat flux from the fluid layer is given by

$$F = \rho c J (T - T_1)^{\frac{3}{2}}, \quad (18)$$

where ρ , c and J have the same meaning as in §2. We assume that the melt layer thickness a grows sufficiently slowly that it is always significantly less than the lengthscale of thermal diffusion $(\kappa_m t)^{\frac{1}{2}}$, where κ_m is the thermal diffusivity of the melt. We can then use a linear conductive profile to describe the temperature in the melt. The conductive flux through the melt is then given by

$$F_m = \frac{k_m (T_1 - T_m)}{a}, \quad (19)$$

where k_m is the thermal conductivity of the melt. The equations for conservation of heat in the fluid layer of thickness D , across the melt/fluid interface and at the solid/melt interface then become

$$\rho c D \dot{T} = -F, \quad (20)$$

$$F = F_m \quad (21)$$

and

$$\dot{a} = \frac{F_m}{H_s}. \quad (22)$$

The initial conditions

$$T = T_0, \quad T_1 = T_m, \quad a = 0 \quad (t = 0) \quad (23a, b, c)$$

complete the specification of the problem.

Substituting (20) and (21) into (22), and using (23a, c) in taking the first integral of the result, we obtain

$$a = \rho c D H_s^{-1} (T_0 - T). \quad (24)$$

Substituting (18), (19) and (24) into (21), we obtain the following implicit relationship between T and T_1 :

$$T_1 = T_m + \rho^2 c^2 k_m^{-1} D J H_s^{-1} (T_0 - T) (T - T_1)^{\frac{3}{2}}. \quad (25)$$

Finally, (18) and (20) can be written

$$\dot{T} = -\frac{J}{D}(T-T_1)^{\frac{4}{3}}. \quad (26)$$

To obtain solutions of (23)–(26), it is convenient to introduce the non-dimensional variables θ , ϕ , η and ω defined by

$$\theta = \frac{T-T_m}{T_0-T_m}, \quad (27a)$$

$$\phi = \frac{T_1-T_m}{T_0-T_m}, \quad (27b)$$

$$\eta = \frac{H_s a}{\rho c D(T_0-T_m)} \quad (27c)$$

and

$$\omega = JD^{-1}(T_0-T_m)^{\frac{1}{3}}t. \quad (27d)$$

The equations then become

$$\frac{d\theta}{d\omega} = -(\theta-\phi)^{\frac{4}{3}}, \quad (28)$$

$$\phi = \beta(1-\theta)(\theta-\phi)^{\frac{4}{3}}, \quad (29)$$

$$\eta = 1-\theta \quad (30)$$

and

$$\theta = 1 \quad (\omega = 0), \quad (31)$$

where

$$\beta = \rho^2 c^2 k_m^{-1} DJH_s^{-1}(T_0-T_m)^{\frac{4}{3}}. \quad (32a)$$

$$= \gamma \frac{\rho c}{\rho_s c_s} \frac{k}{k_m} \frac{T_0-T_m}{T_m-T_\infty + Lc_s^{-1}} Ra_{\text{init}}^{\frac{1}{3}}, \quad (32b)$$

in which k is the thermal conductivity of the fluid and Ra_{init} the initial Rayleigh number of the hot fluid bounded above by the base of the infinitesimally thin melt layer at temperature T_m , viz.

$$Ra_{\text{init}} = \frac{\alpha g(T_0-T_m) D^3}{\kappa \nu}. \quad (33)$$

Figure 8 graphs the relationship (29) between θ and ϕ for various values of β .

For general β these equations need to be solved numerically. However, incorporated into the analysis is the requirement that $Ra_{\text{init}} \gg 1$; from (32b) it is thus reasonable to assume that $\beta \gg 1$ also. For example, values of β in the laboratory experiments or in magma chambers are typically in excess of 10^2 . Making the approximation $\beta \gg 1$ in (28)–(31) allows an analytic solution to be obtained. With $\beta \gg 1$, (29) shows that the difference between θ and ϕ is small and can be represented as

$$\theta - \phi = \epsilon = \beta^{-\frac{3}{4}} \left(\frac{\theta - \epsilon}{1 - \theta} \right)^{\frac{3}{4}} \quad (34a, b)$$

$$= \beta^{-\frac{3}{4}} \left(\frac{\theta}{1 - \theta} \right)^{\frac{3}{4}} [1 + O(\beta^{-\frac{3}{4}})] \quad (35)$$

except near $\theta = 1$, where

$$\theta = 1 - \beta^{-1} \phi(1-\phi)^{-\frac{4}{3}} + O(\beta^{-2}). \quad (36)$$

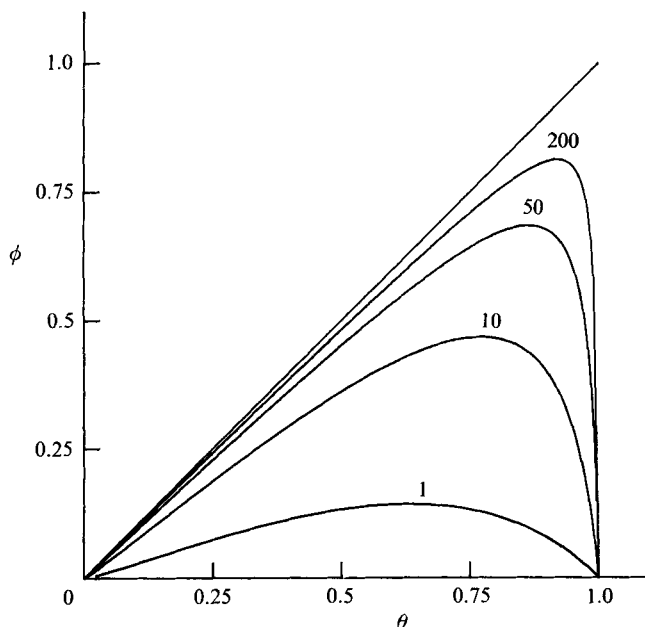


FIGURE 8. The form of ϕ as a function of θ for $\beta = 1, 10, 50$ and 200 .

The physical interpretation of $\theta \approx \phi$ for large β is as follows. For the same temperature differences, convective fluxes are much larger than conductive fluxes. But the convective flux out of the fluid must equal the conductive flux in the melt layer. This can only be so if the temperature difference driving the convection, $T - T_1$, is very much less than that driving the conduction, $T_1 - T_m$. In other words $T_1 \approx T$, so that $\theta \approx \phi$.

This approximation can be used to derive an analytical relationship between ω and θ . Substituting (35) into (28) and integrating the result using (31), we obtain

$$\beta^{-1} \omega = \theta - \ln \theta - 1, \quad (37)$$

which shows that the correct timescale for large β is not $DJ^{-1}(T_0 - T_m)^{-\frac{1}{2}}$ as suggested by (27d), but β times this, as indicated by (37). Figure 9 presents a graph of (37). Also graphed is the relationship between θ and ω obtained by numerical integration of (28)–(31) for smaller values of β .

The above analysis and physical explanation suggests that one could proceed, albeit heuristically, by rearranging (25) and using $T_1 \approx T$ to obtain

$$(T - T_1)^{\frac{3}{2}} = \frac{H_s k_m T - T_m}{\rho^2 c^2 D J T_0 - T}. \quad (38)$$

Substitution of (38) into (26) and integration using (23a) leads directly to (37) expressed in dimensional terms.

Conduction in the melt layer continues until the Rayleigh number for the melt layer,

$$Ra_m = \frac{\alpha_m g (T_1 - T_m) a^3}{\kappa_m \nu_m} \quad (39a)$$

$$= \frac{\alpha_m g \rho^3 c^3 D^3 (T_0 - T_m)^4}{\kappa_m \nu_m H_s^3} (1 - \theta)^3 \phi, \quad (39b)$$

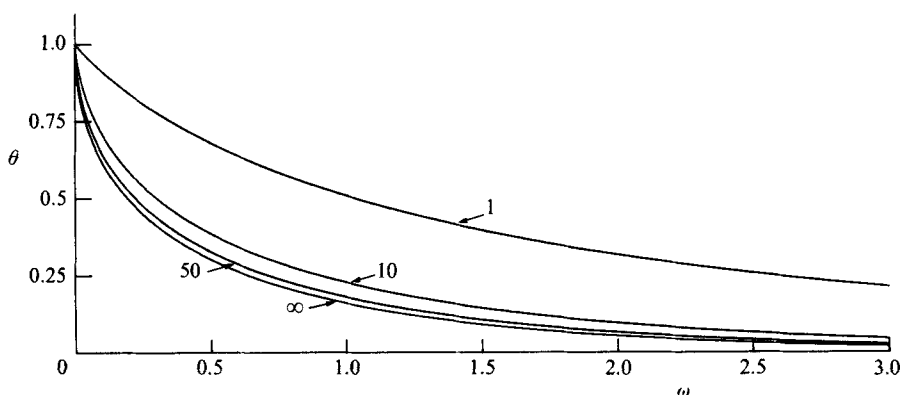


FIGURE 9. The graph of θ as a function of ω for the same values of β as in figure 8 and the asymptotic limit for $\beta \gg 1$ as defined by equation (37).

exceeds a critical value, whose magnitude is probably of order 10^3 . Convection in the melt layer is then initiated and (18) needs to be altered. It is possible that Ra_m , which is small both initially and after a long time, never exceeds the critical value. A melt layer of temperature T_m and thickness $\rho c DH_s^{-1}(T_0 - T_m)$ above a fluid layer at temperature T_m would then be the final state. This would then cool and solidify entirely by conduction.

Generally, however, convection in the melt layer will set in. Initially the convection will be weak. As the layer thickness increases, however, the convection may become sufficiently strong to produce a turbulent layer of uniform temperature, for which the transfer of heat can be described by the four-thirds expression. For illustration we now analyse this strongly turbulent case. A similar analysis of convection at intermediate Rayleigh numbers would require an exact evaluation of the critical Rayleigh number and use of a modified heat-flux relationship until the four-thirds expression became valid.

Consider the situation sketched in figure 7(b). The temperature of the lower, hot fluid layer is denoted by $T(t)$ and that of the melt layer of thickness $a(t)$ by $T_2(t)$. The heat flux from the hot fluid layer is given by

$$F = \rho c J (T - T_1)^{\frac{4}{3}}, \quad (40)$$

where T_1 is the interfacial temperature between the melt and the fluid. The flux from the base of the melt layer, F_B , is given by

$$F_B = \rho_2 c_2 J_2 (T_1 - T_2)^{\frac{4}{3}}, \quad (41)$$

where a subscript 2 indicates that properties of the melt layer are involved. Since by conservation of heat $F = F_B$,

$$T_1 = \frac{T + P T_2}{1 + P}, \quad (42)$$

where

$$P = \left(\frac{\rho_2 c_2 J_2}{\rho c J} \right)^{\frac{3}{4}}. \quad (43)$$

Conservation of heat in the two layers requires further that

$$\rho c D\dot{T} = -F, \quad (44)$$

$$\rho_2 c_2 \frac{d}{dt} [a(T_2 - T_m)] = F_B - F_2 \quad (45)$$

and conservation of heat in the solid requires

$$\dot{a} = \frac{F_2}{H_s}, \quad (46)$$

where

$$F_2 = \rho_2 c_2 J_2 (T_2 - T_m)^{\frac{4}{3}}. \quad (47)$$

The nonlinear system represented by (40)–(47) requires numerical computation for its solution. Results obtained in this way are presented in the next section. A useful analytic solution can be obtained, however, by supposing, subject to *a posteriori* verification, that both F_B and F_2 greatly exceed $\rho_2 c_2 (d/dt)[a(T_2 - T_m)]$. This states that most of the heat flux into the base of the lower layer departs through the top, and a negligible amount is used to change the temperature of the melt layer.

Substitution of (41), (42) and (47) into the relationship $F_B = F_2$ leads to

$$T_2 = \frac{T + (1+P)T_m}{2+P}. \quad (48)$$

Substituting (40), (42) and (48) into (44), we obtain

$$D\dot{T} = -J \left(\frac{P}{2+P} \right)^{\frac{4}{3}} (T - T_m)^{\frac{4}{3}}, \quad (49)$$

which has the solution

$$T = T_m + [Q + R(t - t_1)]^{-3}, \quad (50)$$

where

$$Q = [T(t_1) - T_m]^{-\frac{1}{3}}, \quad (51)$$

$$R = \frac{1}{3} D^{-1} J \left(\frac{P}{2+P} \right)^{\frac{4}{3}} \quad (52)$$

and $T(t_1)$ is the temperature of the hot fluid layer at time t_1 . Substituting (47), (48) and (50) into (46), we obtain a differential equation for a , the solution to which is

$$a = a_1 + \frac{1}{3} \rho_2 c_2 J_2 R^{-1} (2+P)^{-\frac{4}{3}} H_s^{-1} \{Q^{-3} - [Q + R(t - t_1)]^{-3}\}, \quad (53)$$

where $a(t_1) = a_1$. As $t \rightarrow \infty$, T and $T_2 \rightarrow T_m$ while

$$a \rightarrow a_1 + \frac{1}{3} \rho_2 c_2 J_2 Q^{-3} R^{-1} (2+P)^{-\frac{4}{3}} H_s^{-1}.$$

The conditions under which

$$F_B, F_2 \gg \rho_2 c_2 \frac{d}{dt} [a(T_2 - T_m)]$$

are now easily obtained. From (44) and (48)

$$F_B = -\rho c D (2+P) \dot{T}_2. \quad (54)$$

Comparing (54) with (45), we see that the approximation is valid if

$$a \ll \frac{\rho c}{\rho_2 c_2} (2+P) D. \quad (55a)$$

Considering that, typically, $\rho c \approx \rho_2 c_2$ and $P \approx 1$, we can write (55a) as

$$a \ll D. \quad (55b)$$

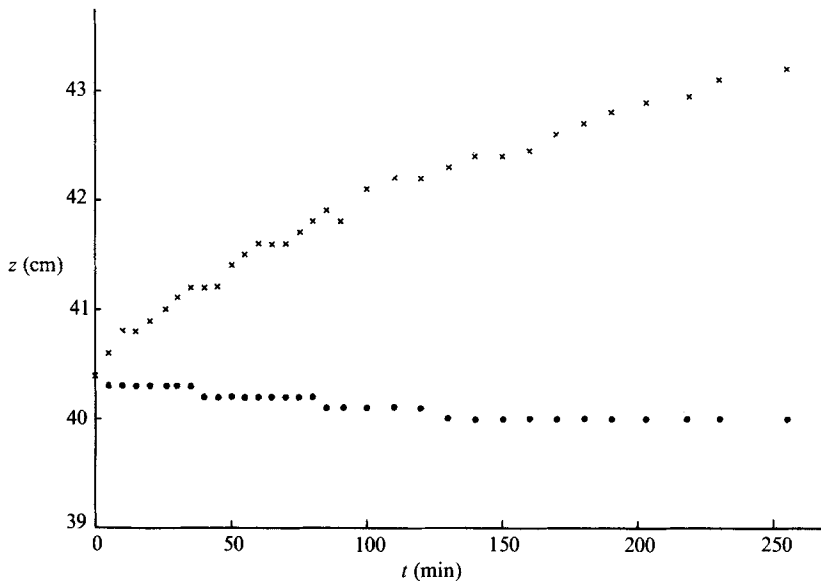


FIGURE 10. Experimental data on the heights of the solid/melt interface (\times) and the melt/fluid interface (\bullet) as functions of time during experiment 2.

From (42), the second condition is that

$$H_s \gg \rho_2 c_2 (T_2 - T_m), \quad (56)$$

which requires that the heat needed to bring the solid to its melting temperature and then to melt it should greatly exceed the heat necessary to subsequently bring it to the mean temperature of the melt layer. When these inequalities are not satisfied, numerical integration of the equations is necessary.

The experiments

We conducted three experiments, as seen in figure 4, in which the melt was always less dense than the fluid. Since then, broadly similar experiments have been reported by Campbell & Turner (1987). The effects observed in both sets of experiments were consistent with the processes already outlined. Figure 10 presents data on the position of the base of the wax and on the position of the fluid/melt interface for experiment 2. There appears to be a slight change of 3 mm over 3 hr in the height of the interface, but this is due mainly to the contraction of the lower layer on cooling. Figure 11 presents the temperature data from the same experiment at different times. The gradual build-up of a uniform temperature in the melt layer as the Rayleigh number increases to a value of approximately 10^5 after 8 hr (due mainly to the increase in thickness of the layer) is clearly evident. This evolution is in qualitative agreement with the behaviour predicted by the theoretical model. Unfortunately, for a significant part of the time the melt layer was not in vigorous turbulent motion and the relationships (50)–(54) would not describe the evolution accurately. Thus, a detailed comparison between theory and experiment was not carried out. The turbulent model would only be applicable to experiments on a much larger scale. Alternatively, a theoretical model to describe the experiments performed would have to incorporate the (unknown) critical Rayleigh number, the initial convective effects at lowish Rayleigh numbers and the influence of the variation of physical properties, such as viscosity.

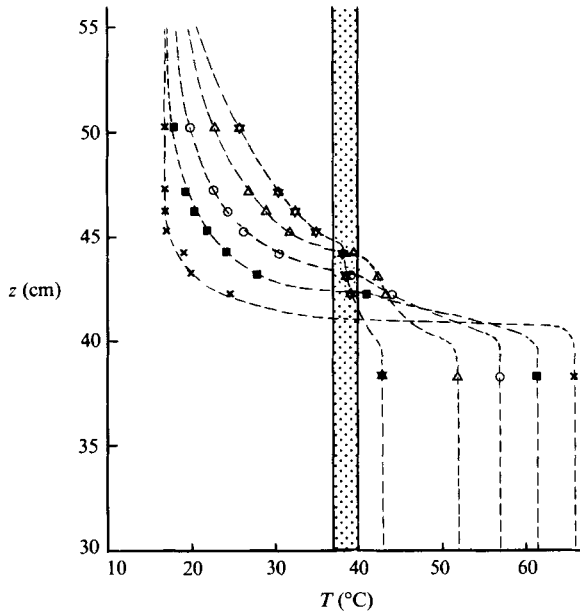


FIGURE 11. Temperature data against height for experiment 2: \times , 30 min; \square , 2 h; \circ , 4 h; \triangle , 8 h; $*$, 20 h.

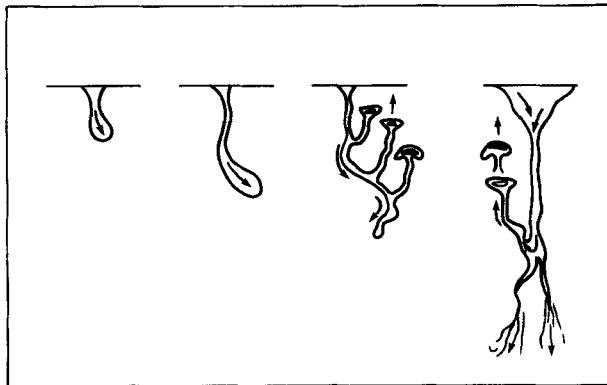


FIGURE 12. Artist's sketches of the formation of light blobs of melt observed during experiments 5 and 6. The first three sketches show a typical development with time and the last sketch is another representation.

4. Melt of intermediate density

In two of the experiments, numbers 5 and 6, the wax at its melting temperature was slightly more dense than the hot fluid and sank. As it did so its temperature increased and its density correspondingly decreased. This decrease could be sufficient to make parts of the molten wax less dense than the surrounding fluid, causing it to rise. Figure 1(c) is a photograph taken during experiment 5 and figure 12 represents artist's sketches of the different flow patterns. The form of motion was similar to the upward-moving blobs observed during various investigations in which light fluid was released beneath heavier fluid (see, for example, Whitehead & Luther 1975; Marsh 1979; Kerr & Lister 1988).

5. Some geological extensions

Volcanism in the Earth can be understood in terms of plate tectonics and convection within the mantle. The upper mantle is close to its solidus temperature and melts to form basalt at three major locations: at mid-ocean ridges, where plates are formed; at those zones where rising hot jets in the mantle impinge upon the plates; and at subduction zones, where plates are destroyed. At the first two sites the decrease of pressure as material rises in the mantle causes substantial melting (McKenzie 1984). At the third, convective motions in the mantle are combined with shear heating and release of water from the subducted plate to reduce the solidus temperature of the mantle. This also causes melting and production of basaltic magma, which contains roughly 50% silica and has a density of about 2.7 g cm^{-3} . The temperature of molten basalts within the Earth covers the range of roughly 1100–1200 °C, with the specific figures depending on the exact composition of the basalt. Below approximately 1100 °C basalts are essentially solid.

In continental regions the uppermost 20–30 km of the plate is largely composed of low-density rocks ($2.3\text{--}2.5 \text{ g cm}^{-3}$), which are rich in silica (typically 65 to 70%) and which melt to form granite magmas. When plate boundaries or hot-spots occur within continents or at continental margins, basalt generated in the mantle invades the continental crust and provides a potent heat source for melting and granite generation. Rocks of the continental crust typically melt to form granite at temperatures between 750 and 900 °C. Because of its higher silica content, the viscosity of a granite melt exceeds that of a molten basalt at the same temperature by several orders of magnitude. In addition, because the viscosity of a magma increases sharply with decreasing temperature, the viscosity of a molten granite can be several orders of magnitude larger than that of a molten basalt.

Various geological observations are consistent with the idea that the basalt is generated in the Earth's mantle and then rises towards the Earth's surface because it is less dense than the surrounding rocks. The melt can then be emplaced into the continental crust at a magma chamber or sill (a horizontal sheet). The hot basalt may then melt the surrounding granite. Subsequently molten granite or molten basalt may be erupted onto the Earth's surface. Alternatively, the molten rocks can slowly cool and solidify within the Earth to form bodies known as plutons.

The present study was motivated by a desire to understand quantitatively the generation of granitic rocks by this process. The work already presented discusses some of the fundamental aspects that occur when the solid roof of a chamber or sill is melted by underlying hot fluid. This section briefly explains how some of the ideas need to be extended in order to be applicable to the geological situation. The main ideas will be presented, though the description is devoid of most of the details, which are explained further in Huppert & Sparks (1988*a, b*).

We simplify the geological geometry somewhat to assume that the molten basalt enters a chamber with horizontal floor and roof of such large extent that processes at the walls may be neglected. The initial temperature of the basalt is assumed to be 1200 °C and the melting point of the granite 850 °C. In fact, the granite has a melting *range*, with some of the minerals melting at lower temperatures than others. At first partial melting will cause the rock to weaken until finally it becomes sufficiently molten to behave as a fluid and to detach from the remaining partially molten solid. The proportion of melt, and hence the temperature, at which this occurs may depend quite strongly on the exact composition of that part of the continental crust under consideration. Empirical evidence indicates that the transition from partially molten

solid to a flowing magma occurs when the proportion of partial melt exceeds about 35% (Marsh 1981). We neglect any effects associated with this melting range by assuming that the melt effectively forms at one specific temperature, where the proportion of partial melt is at the critical value.

The hot basalt will melt both the roof and floor of the chamber. It is suggested that there may be less melting at the floor because of the strongly stabilizing thermal gradient in the magma just above the floor. The current work thus concentrates on the melting of the roof. Because the granite is lighter than the basalt (2.3 g cm^{-3} in contrast to 2.7 g cm^{-3}), the second of the cases discussed above is relevant: the molten granite forms a separate layer above the turbulently convecting basalt.

In the simplest case, we assume that both the basalt and the granite, once molten, cool without any crystallization or solidification and remain at a constant viscosity. We shall call this the 'perfect-fluid' case. For a chamber height of 500 m, a temperature at infinity of 500°C and viscosity of $10^3 \text{ cm}^2 \text{ s}^{-1}$ for the basalt and $1.5 \times 10^6 \text{ cm}^2 \text{ s}^{-1}$ for the granite, the mean temperature of the two layers and the thickness of the granite layer are graphed as dashed curves in figure 13. The growing layer of granitic melt reaches a Rayleigh number of 2000 at 7 days, after which it is assumed to convect turbulently according to the four-thirds relationship. The temperatures of the two layers fall with time, which tends to decrease the Rayleigh number, while at the same time the thickness of the melt layer increases, which tends to increase its Rayleigh number. Initially, it increases and exceeds 10^6 after just over one year. A maximum value of 4.9×10^9 is reached in 105 yr, after which the value decreases. Eventually, the two layers arrive at a common temperature of 850°C , with a melt layer 310 m thick.

However, magmas are not perfect fluids and both basaltic and granitic melts crystallize and increase their viscosity as they cool. From various laboratory experiments (summarized for example by Wyllie 1971), we developed the following empirical relationships for the fraction of crystals x present in a melt as a function of its temperature T :

$$x_b = \frac{7200}{T} - 6 \quad (1091 < T < 1200) \quad (57a)$$

and

$$x_g = \frac{0.65(1000 - T)}{150} \quad (850 < T < 1000), \quad (57b)$$

where the subscripts b and g denote values pertinent to basalt and granite respectively. Above 1000°C granite melts are free of crystals. The very small crystals formed in both basaltic and granitic melts are typically less than 1 mm in size and remain in suspension in the turbulently convecting fluid (Huppert & Sparks 1980; Sparks Huppert & Turner 1984). Thus, in addition to contributing to the heat content of the melt via the latent-heat release, they also increase the viscosity of the melt. Empirical relationships are also available to describe these effects quantitatively (Shaw 1972; Marsh 1981). They are

$$\nu_b = 10^3(1 - 1.67x_b)^{-2.5} \text{ cm}^2 \text{ s}^{-1} \quad (1091 < T < 1200) \quad (58a)$$

and

$$\nu_g = 0.62 \exp \left[\frac{1.8 \times 10^4}{T + 273} \right] (1 - 1.53x_g)^{-2.5} \text{ cm}^2 \text{ s}^{-1} \quad (850 < T < 1000). \quad (58b)$$

These expressions indicate that the increase in viscosity of a cooled basaltic melt depends primarily on the corresponding increase in crystallinity. The effect due to

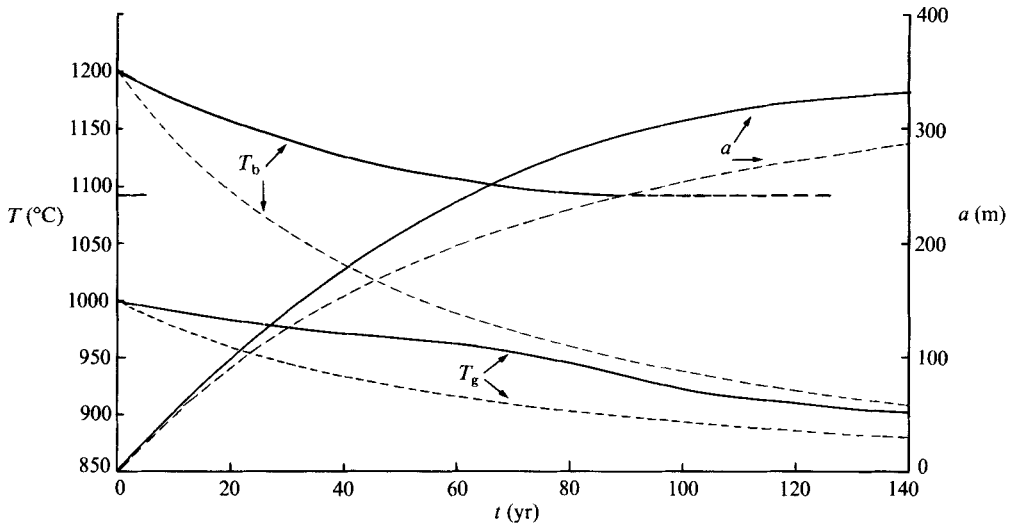


FIGURE 13. The mean temperatures in the basaltic (T_b) and granitic (T_g) layers and the thickness of the granitic layer a as functions of time; ---, perfect-fluid case; —, allowing for crystallization in both layers. The basalt cannot be considered a fluid below 1091 °C.

temperature alone is much smaller, and is neglected in (58a). At a fractional crystallinity of 0.60, which corresponds to a temperature of 1091 °C, the melt is so clogged with crystals that it is effectively a solid. This idea is consistent with the observations that lavas with a fractional crystallinity in excess of 0.60 are rarely sufficiently fluid to be erupted (Marsh 1981). The viscosity of a granitic melt also increases as the temperature decreases, with one factor due directly to temperature alone and another due to crystallinity (which is itself a function of temperature). Beyond a fractional crystallinity of 0.65, attained at a temperature of 850 °C, the granite may be considered solid.

Assuming that the four-thirds heat-flux relationship is unaffected by the presence of the crystals, we can augment the equations for the conservation of heat presented in §3 to incorporate the effects of latent-heat release and include the variation of viscosities in the evaluation of J and J_2 . Typical results are graphed in figure 13. Both the basaltic and the granitic layers cool much more slowly than in the perfect-fluid case, mainly owing to the effects of latent-heat release. Some 15 days after emplacement of the basalt, the granite layer 1.2 m thick, which is above the basalt, begins to convect. A maximum Rayleigh number of 4.0×10^9 is attained in 64 years. After some 90 years the increasing viscosity due to the increasing crystal content becomes paramount in the basaltic layer and it ceases to act as a fluid. Further cooling in the basalt takes place over a timescale of 10^4 years by conduction. The thickness of the granitic melt builds up to a final value of 390 m as its temperature also slowly decreases. When the critical crystallinity is reached (65%) the granite ceases to convect and further cooling takes place by conduction over a timescale of 10^4 years.

A companion paper (Huppert & Sparks 1988a) considers the effects of variations in the temperature of the country rock, the thickness of the basalt layer and the viscosities of the magmas. While these variations cause changes in the numerical results, the general features are unaffected. Calculations for basalt layers with thicknesses from 50 to 1500 m, for example, yield cooling times for the basalt from

25 to 250 years. However, the temperature of the granite melt layer at the time the basalt solidifies hardly changes. As the country-rock temperature is increased above 500 °C more granite is produced, but otherwise there is negligible change in the thermal evolution of both layers.

These calculations give insights into the timescales involved in the generation of granite in the continental crust. Basaltic magma emplaced into the crust as sills cools and crystallizes over periods of only tens of years. The crust melts to form granite magma which cools and crystallizes over periods of only hundreds of years. However, the layer of granite and solidified basalt formed will take of order 10^4 years to cool by conduction back to the original background temperature. The crust as a whole is of order 30 km thick and may take of order 10^6 years to dissipate all the heat input by the emplacement of the basalt sill. Thus melting and crystallization of the magma takes a much shorter time than the time taken to either heat up or cool down the crust.

The calculations thus suggest a conceptual model for the generation of granite magmas during active tectonic periods when basalt is emplaced into the crust. Repeated injections of basalt warm up the crust and eventually the crust is sufficiently hot that each intrusion triggers a short-lived melting event. Such an event may sometimes be associated with intrusions of buoyant granite at higher levels in the crust or eruptions at the surface. Magma bodies would only be transient features over rather short time periods (tens or hundreds of years) after a melting event, in comparison with the thermal relaxation time of the crust after a single or a series of intrusive events. At times between intrusions, the crust in the source region will be either partially molten or close to the melting temperature.

Specific application of these ideas has been made to the volcanic system of the Cerro Galan in Northwestern Argentina. A detailed discussion of the pertinent observations and their interpretation appears in Francies *et al.* (1988).

In conclusion, we remind the reader that we have developed simple theoretical models for the melting of a solid roof by an adjacent turbulent flow. We have also carried out laboratory experiments which have illustrated the main fluid-dynamical processes. One of the aims of our research is to extend these fundamental ideas to analyse the more complicated situations found in geological systems and to aid in the interpretation of geological rock suites.

We are very grateful to Mark Hallworth who helped us with all the experiments and Joyce Wheeler who carried out most of the numerical programming. Professor B. D. Marsh shared some of his recent ideas with us during stimulating conversations which led to the material in the Appendix. Earlier drafts of the manuscript were read and commented upon by P. Bruce, J. Lister and M. G. Worster, to whom we are indebted. Our research is supported by grants from the BP Venture Research Unit and the NERC.

Appendix. The case with no melting

For comparison, this Appendix analyses the situation when the roof does *not* melt. The physical motivation behind the analysis is to determine quantitatively the restraining effect on the turbulent convection of the overlying solid which transfers heat by conduction. The geological motivation is to evaluate the influence of the overlying solid rock both on the heat transfer from the liquid in a magma chamber and on the state of convection in the liquid.

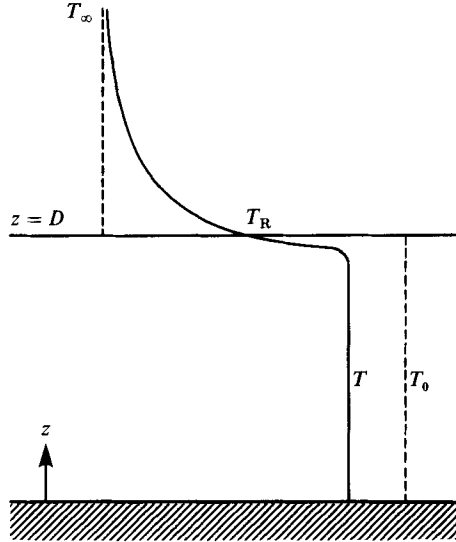


FIGURE 14. A sketch of the geometry and mean temperature profile when the roof does not melt.

Consider fluid of initial temperature T_0 to be introduced at $t = 0$ into a horizontal layer of depth D . The layer is assumed to be thermally insulated at its base and to transfer heat by turbulent convection to the semi-infinite solid above, whose initial temperature is T_∞ and whose temperature always tends to T_∞ in the far field, as sketched in figure 14. Denote the temperature at the roof by $T_R(t)$ with $T_R(0) = T_\infty$. The (time-dependent) Rayleigh number of the system Ra is given by

$$Ra = \frac{\alpha g (T - T_R) D^3}{\kappa \nu}, \quad (\text{A } 1)$$

where T is the mean temperature of the fluid layer; its initial value is

$$Ra_0 = \frac{\alpha g (T_0 - T_\infty) D^3}{\kappa \nu}. \quad (\text{A } 2)$$

On the assumption that the Rayleigh number remains sufficiently large that the fluid continues to convect turbulently, we seek to determine T , T_R and hence Ra as functions of time.

We assume that the heat transfer from the fluid to the solid is given by

$$F = \rho c J (T - T_R)^{\frac{3}{2}}. \quad (\text{A } 3)$$

Then a standard result in Carslaw & Jaeger (1959, p. 76 (9)), which relates the temperature in a semi-infinite solid to the heat flux incident at the boundary, can be used to determine the following integral equation for T_R :

$$T_R(t) = T_\infty + \frac{\rho c}{\rho_s c_s (\pi \kappa_s)^{\frac{1}{2}}} \int_0^t \frac{[T(\lambda) - T_R(\lambda)]^{\frac{3}{2}}}{(t - \lambda)^{\frac{1}{2}}} d\lambda, \quad (\text{A } 4)$$

where ρ_s, c_s and κ_s are the density, specific heat and thermal diffusivity of the solid. The heat flux from the fluid causes it to cool according to

$$\dot{T} = -\frac{J}{D}(T - T_R)^{\frac{4}{3}}. \quad (\text{A } 5)$$

We seek the solution of the integro-differential system (A 4) and (A 5) together with the boundary conditions

$$T = T_0, \quad T_R = T_\infty \quad (t = 0). \quad (\text{A } 6a, b)$$

It is convenient to introduce non-dimensional temperatures θ and θ_R and time τ by

$$T(t) = T_\infty + (T_0 - T_\infty)\theta(\tau), \quad (\text{A } 7a)$$

$$T_R(t) = T_\infty + (T_0 - T_\infty)\theta_R(\tau) \quad (\text{A } 7b)$$

and

$$t = \frac{D\tau}{J(T_0 - T_\infty)^{\frac{1}{3}}}. \quad (\text{A } 7c)$$

In terms of these variables, the integro-differential system becomes

$$\theta_R(\tau) = \Gamma \int_0^\tau \frac{[\theta(\lambda) - \theta_R(\lambda)]^{\frac{4}{3}}}{(\tau - \lambda)^{\frac{1}{2}}} d\lambda, \quad (\text{A } 8a)$$

$$\theta'(\tau) = -(\theta - \theta_R)^{\frac{4}{3}} \quad (\text{A } 8b)$$

$$\theta(0) = 1, \quad \theta_R(0) = 0, \quad (\text{A } 8c, d)$$

where

$$\Gamma = \frac{\rho c}{\rho_s c_s} \left(\frac{DJ}{\pi k_s} \right)^{\frac{1}{2}} (T_0 - T_\infty)^{\frac{1}{6}} \quad (\text{A } 9a)$$

$$= \frac{\rho c}{\rho_s c_s} \left(\frac{\gamma \kappa}{\pi \kappa_s} \right)^{\frac{1}{2}} Ra_0^{\frac{1}{6}}. \quad (\text{A } 9b)$$

We proceed under the assumption that $\Gamma \gg 1$. The system (A 8) then has a short-time solution which can be expressed in terms of the short-time variable τ_s given by

$$\tau_s = \Gamma^2 \tau. \quad (\text{A } 10)$$

The leading-order solution is

$$\theta(\tau_s) = 1 \quad (\text{A } 11a)$$

$$\theta_R(\tau_s) = \int_0^{\tau_s} \frac{[1 - \theta_R(\lambda)]^{\frac{4}{3}}}{(\tau_s - \lambda)^{\frac{1}{2}}} d\lambda, \quad (\text{A } 11b)$$

$$\rightarrow 1 \quad (\tau_s \rightarrow \infty), \quad (\text{A } 11c)$$

where $\theta_R(\tau_s)$ needs to be evaluated numerically and is graphed in figure 15.

Physically, (A 11) states that on the short timescale of $t_s = \Gamma^{-2}D/(J(T_0 - T_\infty)^{\frac{1}{3}})$, the temperature in the body of the fluid does not change, while the temperature at the roof builds up to be (at leading order) equal to that of the fluid. Were it to become exactly equal, convection would cease; but it always remains just a little less, by an amount that can be evaluated by investigating the long-time solution.

This is most conveniently analysed in terms of the long-term variable τ_L given by

$$\tau_L = \Gamma^{-2}\tau \quad (\text{A } 12)$$

and by substituting

$$\theta(\tau_L) = \theta_R(\tau_L) + \Gamma^{-\frac{3}{2}}f(\tau_L) \quad (\text{A } 13)$$

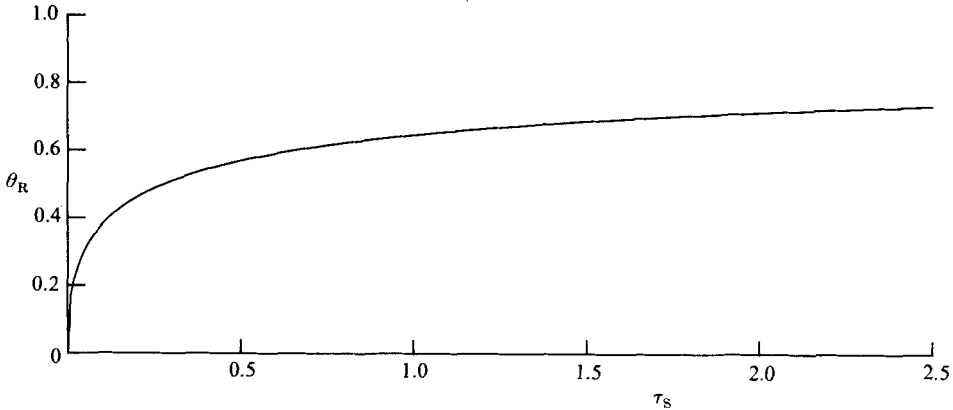


FIGURE 15. The non-dimensional temperature of the roof $\theta_R = (T_R - T_\infty)/(T_0 - T_\infty)$ as a function of the non-dimensional short-time variable $\tau_s = J(T_0 - T_\infty)^{1/3} D^{-1} \Gamma^{-2} t$.

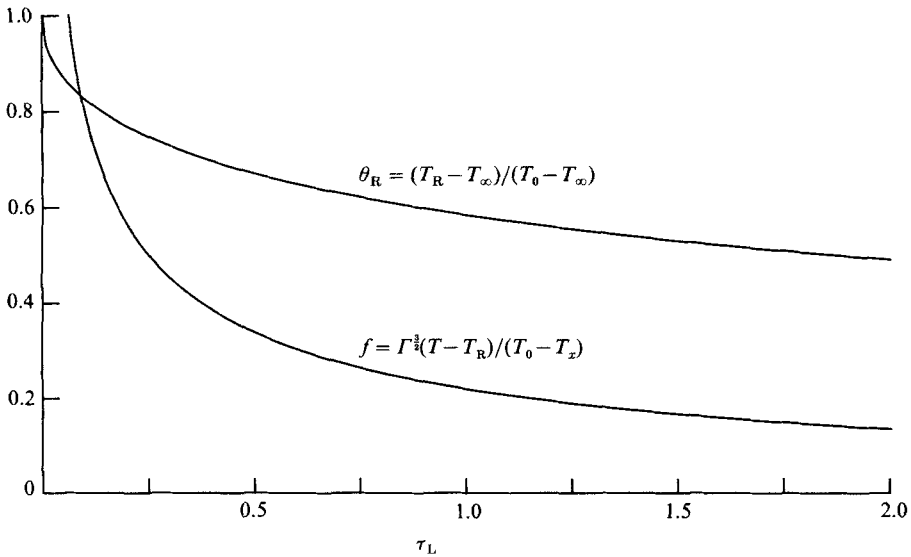


FIGURE 16. The non-dimensional temperature of the roof θ_R and temperature difference between roof and contained fluid f , as functions of the non-dimensional, long-time variable $\tau_L = J(T_0 - T_\infty)^{1/3} D^{-1} \Gamma^2 t$.

into (A 8a, b). The result, after combining the two equations, is

$$\theta_R(\tau_L) = - \int_0^{\tau_L} \frac{\theta'_R(\lambda)}{(\tau - \lambda)^{1/2}} d\lambda, \tag{A 14a}$$

$$\theta_R(0) = 1, \tag{A 14b}$$

the boundary condition (A 14b) being required to match the short-time limit at ∞ expressed by (A 11c). Equations (A 14) can be solved by a standard application of the techniques of Laplace transforms to yield

$$\theta_R(\tau_L) = e^{(\tau_L/\pi)} \operatorname{erfc} [(\tau_L/\pi)^{1/2}], \tag{A 15}$$

and

$$f(\tau_L) = \{\pi^{-1} [\tau_L^{-1/2} - \theta_R(\tau_L)]\}^{3/4}. \tag{A 16}$$

Figure 16 graphs both these functions.

	Typical value in the laboratory	Typical value in a magma chamber
Ra_0	10^{11}	10^{15}
$Ra_0^{\frac{3}{4}}$	10^8	10^{11}
Γ	4	200
t_s	200 s	100 s
t_m	40 min	50 days
t_L	10 h	4000 years

TABLE 1. Typical values in the laboratory and in nature of the initial Rayleigh number and the three relevant timescales

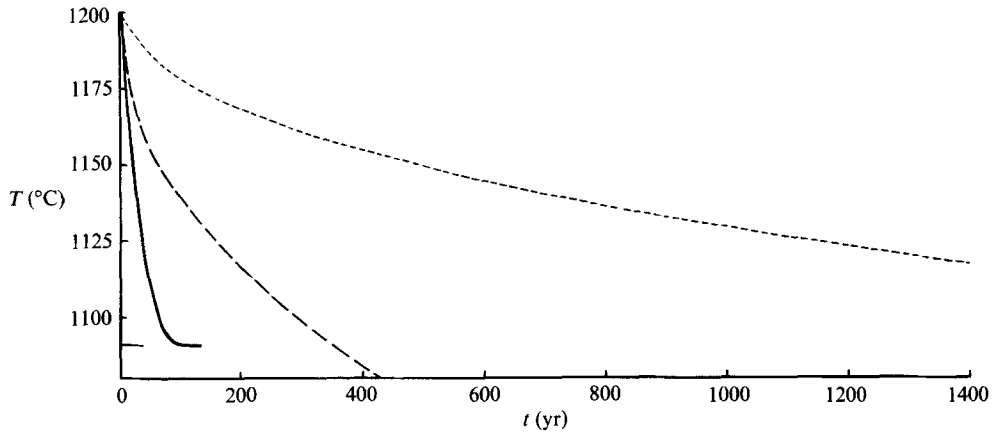


FIGURE 17. The temperature of a contained basalt as a function of time: ---, the basalt is considered as a perfect fluid and no melting is allowed; — · —, the basalt is allowed to crystallize but the roof does not melt; —, the basalt crystallizes and the roof melts just as in figure 13.

Physically, this solution states that after the short timescale t_s the temperature of the fluid exceeds that at the roof by an amount of order $\Gamma^{\frac{3}{4}}$. This decreases the effective Rayleigh number to

$$Ra = \frac{\alpha g \Gamma^{\frac{3}{4}} (T_0 - T_\infty) D^3 f(\tau_L)}{\kappa \nu} \quad (\text{A } 17a)$$

$$= \left(\frac{\rho c}{\rho_s c_s} \right)^{-\frac{3}{4}} \left(\frac{\gamma \kappa}{\pi \kappa_s} \right)^{-\frac{3}{4}} Ra_0^{\frac{3}{4}} f(\tau_L). \quad (\text{A } 17b)$$

The fluid will continue to convect turbulently and the four-thirds expression (A 3) remain valid provided Ra exceeds a value of about 10^6 . It is interesting to note that the initial Rayleigh number appears to the $\frac{3}{4}$ power in (A 17b). Thus, assuming that the first two multiplicative terms in (A 17b) are around 1 and since f is of order unity, the effect of the thermally conducting roof is to reduce the effective Rayleigh number in order of magnitude by the $\frac{3}{4}$ power of its initial value. On the assumption that this is sufficiently large, the fluid continues to transfer heat to the roof by convection over the long timescale $t_L = \Gamma^2 D / [J(T_0 - T_\infty)^{\frac{1}{3}}]$.

Were the roof to be maintained at its initial temperature, the convection would persist over the medium-time scale $t_M = D / [J(T_0 - T_\infty)^{\frac{1}{3}}]$. The initial Rayleigh number

and the three timescales t_S , t_M and t_L are tabulated for typical laboratory and natural systems in table 1.

Figure 17 presents the temperature as a function of time for a fluid with the same values of physical parameters as discussed in §4. Both the perfect-fluid case and the situation in which crystallization occurs are presented. As before, the effect of crystallization is to reduce the thermal decay rate considerably. Also plotted is the geologically realistic case allowing for melting, which has already been plotted in figure 13. It is seen that the melting of the roof enormously increases the thermal decay rate.

REFERENCES

- CAMPBELL, I. H. & TURNER, J. S. 1987 A laboratory investigation of assimilation at the top of a basaltic magma chamber, *J. Geol.* **95**, 155–172.
- CARSLAW, H. S. & JAEGER, J. C. 1959 *Conduction of Heat in Solids*. Oxford University Press.
- DENTON, R. A. & WOODS, I. R. 1979 Turbulent convection between two horizontal plates. *Intl J. Heat Mass Transfer* **22**, 1339–1346.
- FRANCIS, P. W., SPARKS, R. S. J., HAWKESWORTH, C. J., THORPE, R. S., PYLE, D. M. & TAIT, S. R. 1988 Petrology and geochemistry of volcanic rocks of the Cerro Galan caldera, Northwest Argentina. *Geol. Mag.* (sub judice).
- HOLMAN, J. P. 1976 *Heat Transfer*. MacGraw-Hill.
- HUPPERT, H. E. 1986 The intrusion of fluid mechanics into geology. *J. Fluid Mech.* **173**, 557–594.
- HUPPERT, H. E. & SPARKS, R. S. J. 1980 The fluid dynamics of a basaltic magma chamber replenished by influx of hot, dense ultrabasic magma. *Contr. Miner. Petr.* **75**, 279–289.
- HUPPERT, H. E. & SPARKS, R. S. J. 1985 Komatiites I: Eruption and flow. *J. Petr.* **26**, 694–725.
- HUPPERT, H. E. & SPARKS, R. S. J. 1988a The generation of granitic magmas by intrusion of basalt into continental crust. *J. Petr.* (in press).
- HUPPERT, H. E. & SPARKS, R. S. J. 1988b The fluid dynamics of crustal melting by injection of basaltic sills. *Proc. R. Soc. Edin.: Earth Sci.* (in press).
- HUPPERT, H. E., SPARKS, R. S. J., TURNER, J. S. & ARNDT, N. T. 1984 Emplacement and cooling of komatiite lavas. *Nature* **309**, 19–22.
- KERR, R. C. & LISTER, J. R. 1988 Island arc and mid-ocean ridge volcanism, modelled by diapirism from linear source regions. *Earth Planet. Sci. Lett.* (sub judice).
- MCKENZIE, D. P. 1984 The generation and compaction of partially molten rock. *J. Petr.* **95**, 713–765.
- MARSH, B. D. 1979 Island arc development: some observations, experiments and speculations. *J. Geol.* **87**, 687–713.
- MARSH, B. D. 1981 On the crystallinity, probability of occurrence and rheology of lava and magma. *Contr. Miner. Petr.* **78**, 85–98.
- SHAW, H. R. 1972 Viscosities of magmatic liquids: an empirical method of prediction. *Am. J. Sci.* **272**, 870–893.
- SPARKS, R. S. J., HUPPERT, H. E. & TURNER, J. S. 1984 The fluid dynamics of evolving magma chambers, *Phil. Trans. R. Soc. Lond. A* **310**, 511–534.
- TURNER, J. S. 1973 *Buoyancy Effects in Fluids*. Cambridge University Press.
- TURNER, J. S., HUPPERT, H. E. & SPARKS, R. S. J. 1986 Komatiites II: Experimental and theoretical investigations of post-emplacement cooling and crystallization. *J. Petr.* **27**, 397–437.
- WHITEHEAD, J. A. & LUTHER, D. S. 1975 Dynamics of laboratory diapir and plume models. *J. Geophys. Res.* **80**, 705–717.
- WYLLIE, P. J. 1971 *The Dynamic Earth*. Wiley.